Biomass Conversion and Biorefinery (2023) 13:16781–16789
https://doi.org/10.1007/s13399-021-02103-7

ORIGINAL ARTICLE

Activated carbon derived from walnut green peel as an electrode material for high-performance supercapacitors

Na Tian[1] · Man Gao[1] · Xuan-He Liu[1] · Xiaoming Liu[1] · Tiantian Yang[1] · Wenke Xie[1] · Jing Wu[1]

Received: 12 September 2021 / Revised: 29 October 2021 / Accepted: 22 November 2021 / Published online: 7 January 2022

Abstract

How to dispose agricultural waste walnut green peel has been a hard nut to crack during the ripening season. Transforming walnut green peel into activated carbon as electrode materials for energy storage devices would be a potential avenue to reduce the caused environmental pollution. Here, activated porous biomass carbon was successfully prepared by a simple KOH two-step activation of walnut green peel and applied in supercapacitors. Thereinto, the prepared carbon WGL-7 activated at 700 ºC showed high specific surface area (1404.3 $m^2 g^{-1}$), abundant structural defects and pore structure, modest oxygen doping and wettability, and fast charge-transfer. The capacitance of WGL-7 modified electrodes could achieve 236 F g^{-1} at 0.5 A g^{-1} in 6 M KOH electrolyte, and its calculated energy density and power density were 31.8 W h kg^{-1} and 1003.5 W kg^{-1}. The capacitance retention rate remained 94.4% after 3000 cycles at 10 A g^{-1}. These results indicate that walnut green peel-activated carbon as the electrode material of supercapacitor has great capacitive performance.

Keywords Walnut green peel · Biomass · Activated porous carbon · Supercapacitor

1 Introduction

With the rapid development of the economy, the burning of coal and fossil resources has brought problems of environmental pollution and resource shortage. Therefore, it is urgent to find low-cost and green alternative energy [1–4]. Renewable energy sources, composed of wind and solar, tidal, and wave etc. are clean and can be converted into electrochemical energy [5–9]. However, intermittence of these energies endows the development of energy storage devices with significance. As one of them, supercapacitors show the advantages of high powerful density and specific energy, fast charging/discharging, excellent electrochemical stability, and so on [10–14]. Carbon-based materials [15–17], metallic oxides [18, 19], and conductive polymer [20, 21] can be ideal electrode materials. Among them, porous carbon materials show excellent supercapacitor performance because of their high specific surface area, outstanding chemical stability, and developed pore structure [18, 22, 23].

Plant biomass is the only sustainable source of organic carbon for the time being. Therefore, the activated porous carbon materials from plant biomass have attracted much attention [24–30]. In general, specific surface area, aperture distribution, and functional groups on the surface of activated carbon are the main determining factors deciding the performance of their supercapacitors [31–34]. Activated carbon with high specific surface area and abundant aperture structures facilitate ion diffusion. Abundant carboxyl groups and hydroxyl groups benefit the wetting of electrodes [35–37]. The walnut green peel presents a kind of network structure, composed of glucose, naphthoquinones, terpenoids, and polyphenols [38, 39]. And the walnut green peel is rich in carbon elements and oxygen functional groups. This gives a strong hint that walnut green peel is a potential outstanding raw material to prepare activated porous carbon materials as supercapacitor electrodes. In addition, China's annual output of accessible walnut green peel is more than 350,000 tons [40, 41]. Therefore, making good use of walnut green peel is not only economical but also can effectively reduce environmental pollution.

In this paper, walnut green peel was used as the raw material to prepare activated porous carbon in different activation temperatures by direct pyrolysis and KOH activation [25–30]. The intrinsic properties of these activated porous carbons were explored based on their morphology, composition, and pore

✉ Xuan-He Liu
liuxh@cugb.edu.cn

✉ Jing Wu
wujing@cugb.edu.cn

[1] School of Science, China University of Geosciences (Beijing), Beijing 100083, People's Republic of China

structure. Under the optimized annealing temperature, the prepared activated porous carbon showed a high specific surface area of 1404.3 $m^2 g^{-1}$ and was demonstrated to show excellent electrochemical performance with a large specific capacitance (236 F g^{-1} at 0.5 A g^{-1}) in 6.0 M KOH electrolyte in the three-electrode system and had high capacitance retention rate, comparable to the previously reported activated carbons derived from biomass including poultry litter [13], lotus leaf [14], fungal hyphae [16], wheat flour [23], larch [28], tobacco rod [31], lemon peel [34], cotton [42], baobab fruit shell [43], pinecone [44], walnut shell [45], orange peel [46], seaweed [47, 48], onion [48], and rice straw [49]. Table 1 showed their specific capacitance performance.

2 Experimental

2.1 Synthesis of activated porous carbon from walnut green peel

Walnut green peel was collected from the China University of Geosciences, Beijing, then washed, dried, and ground into powder. The walnut green peel powder was calcined under N_2 at 500 °C for 2 h to obtain the optimized pre-carbonization products (Fig. S1). The pre-carbonized walnut green peel powder and KOH were thoroughly mixed at a mass ratio of 1:4. After that, the mixture was heated at 600, 700, and 800 °C for 2 h under N_2/Ar to obtain three different carbonization products named WGL-6, WGL-7, and WGL-8 respectively. The products were rinsed to be neutral (pH = 7) and dried to be used. The synthetic process was displayed in Scheme 1.

2.2 Electrochemical measurement

All electrochemical performance tests were performed on a CHI760E electrochemical workstation using a three-electrode system in 6.0 M KOH electrolyte. Platinum and Hg/HgO electrodes were used as the counter electrodes and reference electrodes, respectively. The working electrodes were prepared by coating WGLs, acetylene black, and PVDF on the nickel foam in a certain proportion.

3 Results and discussion

SEM images in Fig. 1a, d, and h Fig. 2 exhibited the morphology of WGL-6, WGL-7, and WGL-8. WGL-6 and WGL-7 showed a sheet-like morphology and the thickness of WGL-7 nanosheets were ~ 70 nm, while WGL-8 exhibited the agglomerated structure. TEM images further revealed

Table 1 Specific capacitance of reported activated carbon of different biological wastes

Number	Biomass	Main elements	Capacitance value	References
1	Poultry litter	C, O	229 F g^{-1} at 0.2 A g^{-1}	[13]
2	Lotus leaf	C, N, O	353.7 F g^{-1} at 0.5 A g^{-1}	[14]
3	Fungal hypha	C, N, O	279 F g^{-1} at 1 A g^{-1}	[16]
4	Wheat flour	C, O	161.4 F g^{-1} at 0.5 A g^{-1}	[23]
5	Larch	C, O, Si	254.0 F g^{-1} at 0.2 A g^{-1}	[28]
6	Tobacco rod	C, N, O	286.6 F g^{-1} at 0.5 A g^{-1}	[31]
7	Lemon peel	C, O	152.14 F g^{-1} at 10 mV s^{-1}	[34]
8	Cotton	C, O, P	278 F g^{-1} at 1 A g^{-1}	[42]
9	Baobab fruit shell	C, N, O	233.48 F g^{-1} at 1 A g^{-1}	[43]
10	Pinecone	C, O	185 F g^{-1} at 0.5 A g^{-1}	[44]
11	Walnut shell	C, O	169.2 F g^{-1} at 0.5 A g^{-1}	[45]
12	Orange peel	C, N, O	180.2 F g^{-1} at 1 A g^{-1}	[46]
13	Seaweed	C, O, Ca	226.3 F g^{-1} at 10 mV s^{-1}	[47]
14	Onion	C, O	179.5 F g^{-1} at 0.5 A g^{-1}	[48]
15	Rice straw	C, O	150.7 F g^{-1} at 0.1 A g^{-1}	[49]

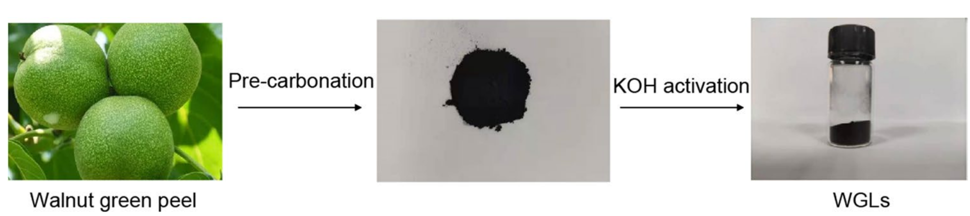

Scheme 1 The schematic diagram for activated carbon WGLs from walnut green peel

the morphology of these carbon materials. TEM images of WGL-6, WGL-7, and WGL-8 were displayed in Fig. 1b, e, and i. The sheet-like morphology with abundant pores can be clearly observed in WGLs. Scattered graphitic structure domains of WGL-7 and WGL-8 can be indicated by obvious graphite layer fringes in high-solution TEM images (Fig. 1f, j), which can facilitate electrical conductivity of carbon materials and charge transfer in supercapacitors. Lattice spacing value of ~ 0.32 nm corresponded to (002) plane of graphite [42]. WGL-6 had no obvious graphite structure domain due to low calcination temperature (Fig. 1c), indicating that its low degree of graphitization element distribution of WGL-7 was investigated by energy dispersive spectrum (EDS) elemental mapping (Fig. 1e–f). Two elements, C (89%) and O (12%), were uniformly distributed in WGL-7.

The crystallite structure of WGL-6, WGL-7, and WGL-8 was demonstrated by X-ray diffraction (XRD) (Fig. 3a). They all showed a broad peak at 20 ~ 30° and a peak at 43°, corresponding to planes (002) and (100) of graphite [50]. The XRD patterns indicated the limited graphitization of WGL-6, WGL-7, and WGL-8. Raman spectra analysis was performed and shown in Fig. 3b. Two significant peaks at ~ 1350 and ~ 1580 cm^{-1} were assigned to D band and G band of carbon [29] and represented structural defects and graphite carbon structure, respectively. The defects in WGL-6, WGL-7, and WGL-8 were evaluated by the calculated relative strength ratio (I_D/I_G). The I_D/I_G values of WGL-6, WGL-7, and WGL-8 were 0.87, 0.91, and 0.93, which demonstrated that all the carbon materials possessed abundant structural defects after activation and calcination. Fourier transform infrared spectroscopy (FT-IR) spectra of WGL-6, WGL-7, and WGL-8 were shown in Fig. 4c . WGLs showed two sharp peaks at ~ 1230 and ~ 1035 cm^{-1}, attributable to the C = O and C–O stretching vibrations [43]. The absorption peaks at ~ 1390 cm^{-1} can be attributed to the –OH to bend vibrations and peaks from ~ 1550 to ~ 1840 cm^{-1} were derived from the C = C and C = C in-plane vibration []. FT-IR results indicated that WGLs had abundant hydroxyl groups and carboxyl groups.

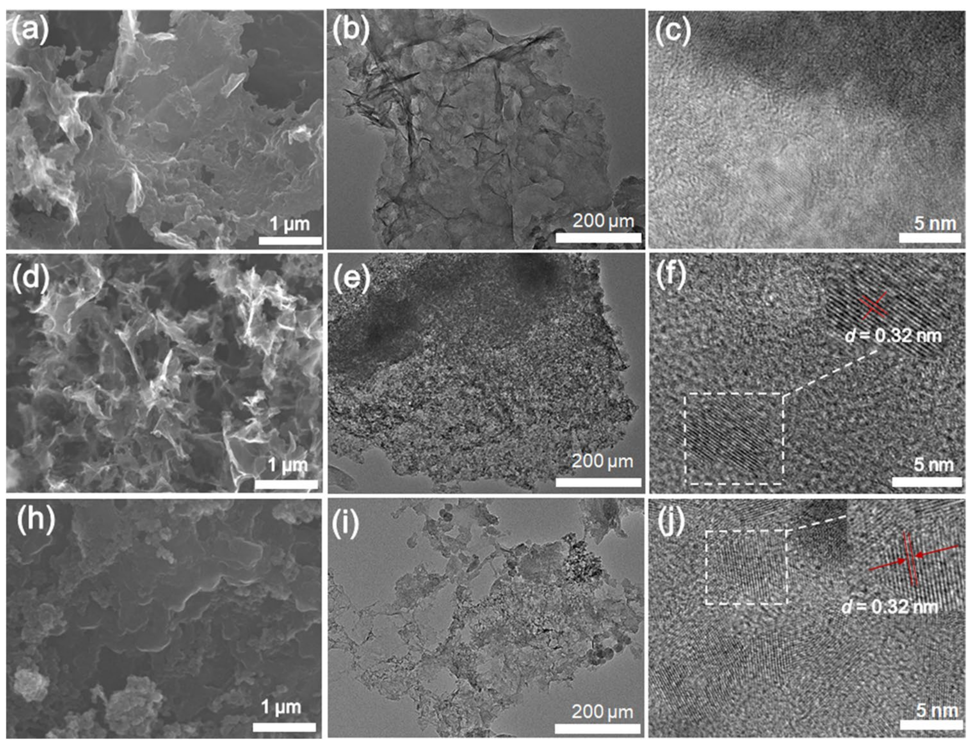

Fig. 1 SEM image (**a**), TEM image (**b**), and HR-TEM image (**c**) of WGL-6; SEM image (**d**), TEM image (**e**), HR-TEM image (**f**) of WGL-7; SEM image (**h**), TEM image (**i**), and HR-TEM image (**j**) of WGL-8

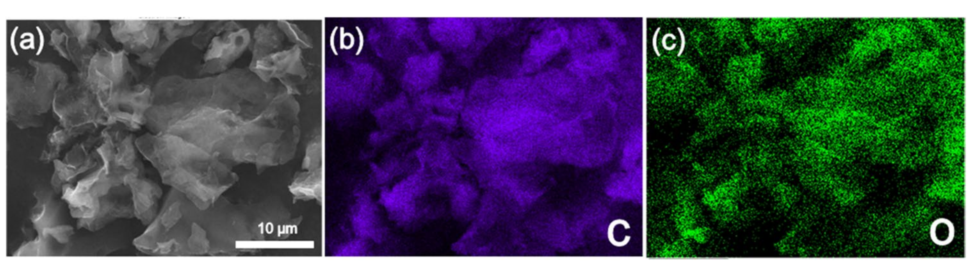

Fig. 2 The elemental mapping images (**a**–**c**) of WGL-7

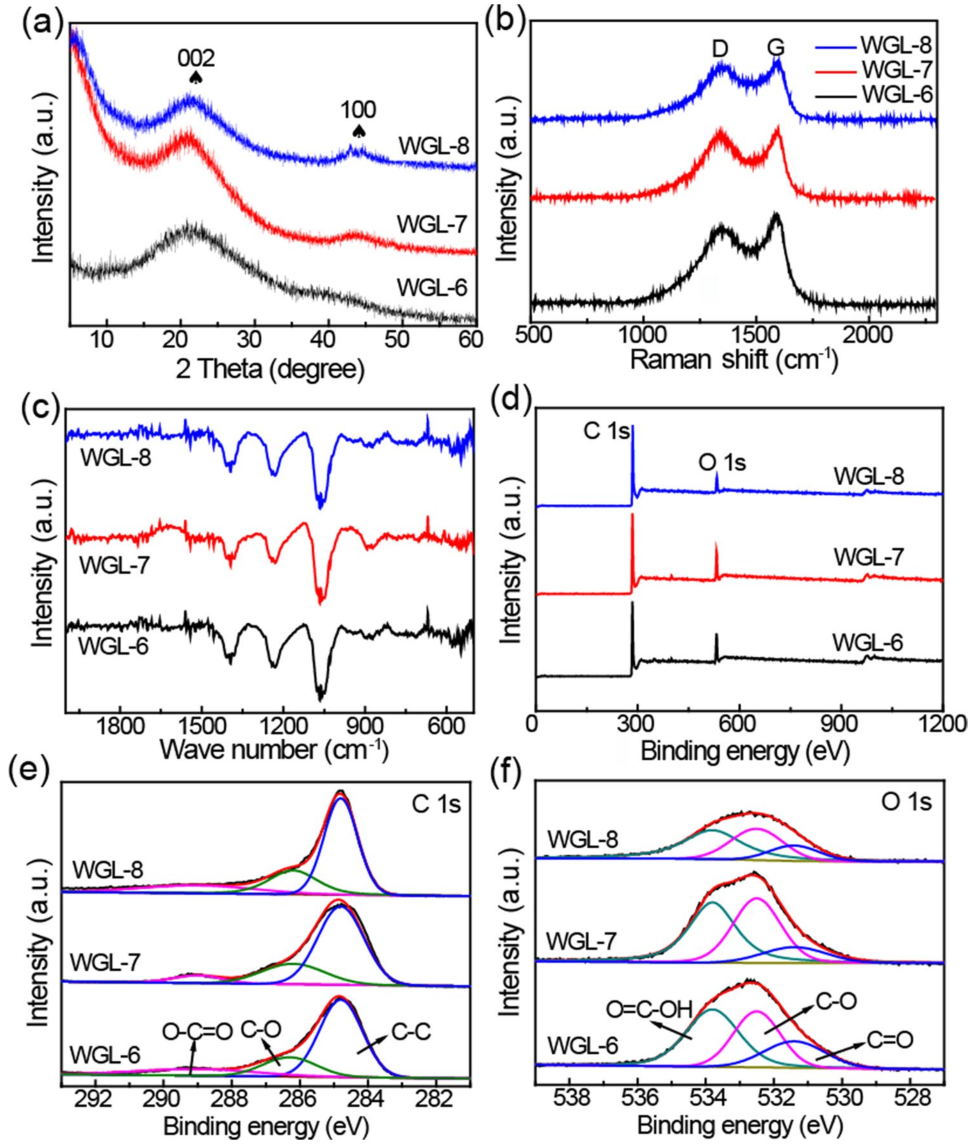

Fig. 3 XRD patterns (**a**), Raman spectra (**b**), Infrared spectra (**c**), XPS survey spectra (**d**), and high-resolution C 1 s (**e**) and O 1 s (**f**) XPS spectra of WGL-6, WGL-7, and WGL-8

The XPS survey spectra of WGL-6, WGL-7, and WGL-8 were shown in Fig. 3d. Only C 1 s and O 1 s peaks without other obvious impurities were observed. High-resolution C 1 s XPS spectra were displayed in Fig. 3e. Three deconvolved peaks at 284.8, 286.2, and 289.0 eV corresponded to C–C, C–O, and C = O, respectively [43, 51]. The O 1 s spectra of WGL-6, WGL-7, and WGL-8 in Fig. 3f can be curve-fitted as three peaks at 531.4, 532.5, and 533.8 eV, which were assigned to element O in bonds of C = O, C–O, and O = C–OH functional groups [43, 51, 52]. The C element contents of WGL-6, WGL-7, and WGL-8 were 85.7%, 87.0%, and 91.5%. And the O contents were 14.3%, 12.9%, and 8.5%, respectively. The element content based on XPS analysis of WGL-7 agreed with the EDS mapping results. It can be concluded that higher activation temperature contributed to the decrease of O content. It was acknowledged that O-functional content played an important role in the surface characteristics of carbon-based materials. Therefore, contact angle tests (Fig. 4) were carried out to investigate their wettability. The contact angles of WGL-6, WGL-7, and WGL-8 showed in Fig. 4 were 111.7°, 112.8°, and 126.4°, respectively. It was demonstrated that porous carbon WGL-6 and WGL-7 with more oxygen-containing functional groups exhibited higher wettability.

To determine the pore texture properties and specific surfaces area of WGL-6, WGL-7, and WGL-8, BET tests were performed. The nitrogen adsorption–desorption isotherms were shown in Fig. 5a. The isotherms exhibited a feature of type I and type IV isotherms, which demonstrated the presence of both micropores and mesopores in WGL-6, WGL-7, and WGL-8 [44, 52, 53]. The corresponding specific surface areas of WGL-6, WGL-7, and WGL-8 were calculated to be 1159.7, 1404.3, and 1067.9 $m^2\ g^{-1}$, respectively. The

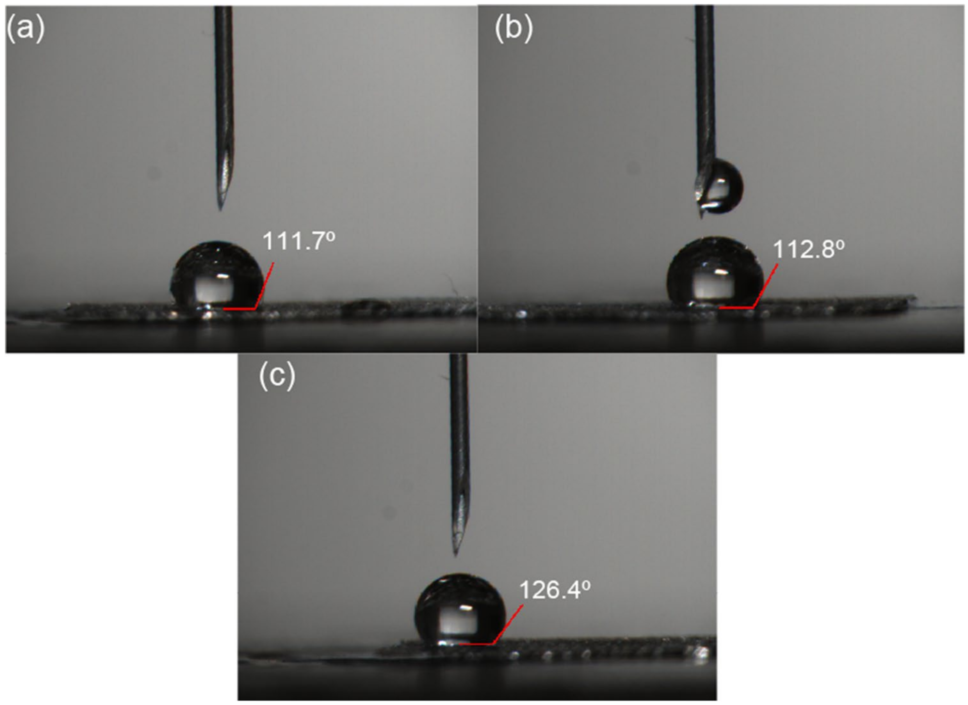

Fig. 4 Contact angle test images of WGL-6 (**a**), WGL-7 (**b**), and WGL-8 (**c**)

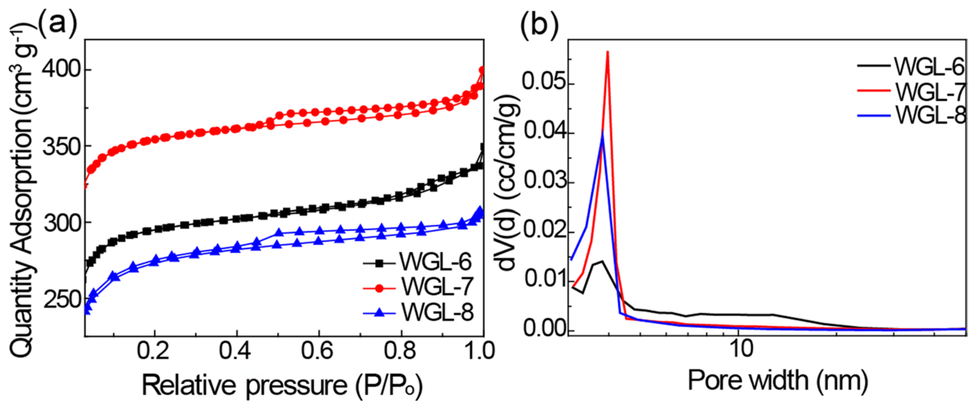

Fig. 5 N_2 adsorption–desorption isotherms (**a**) and pore size distributions (**b**) of WGL-6, WGL-7, and WGL-8

results verified that activation temperature of 700 ℃ showed the highest surface area, which facilitated to enhance the specific capacitance. The pore size distribution (Fig. 5b) calculated by density functional theory (DFT) methods further confirmed the presence of micropores and mesopores in WGL-6, WGL-7, and WGL-8, and the pore size was distributed at mainly between 2 and 10 nm. Based on the BET results, it can be predicted that all WGLs can be potential in

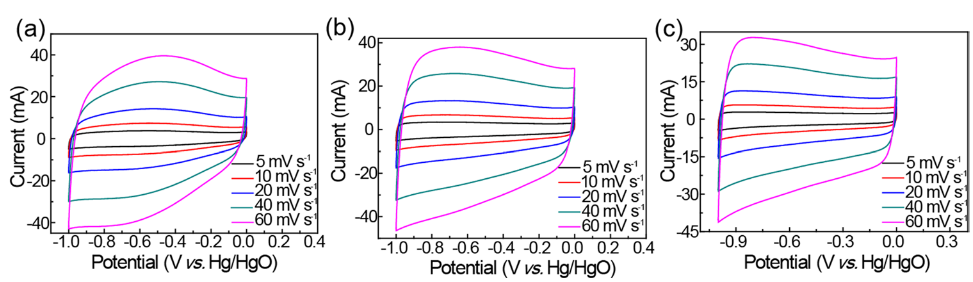

Fig. 6 CV curves of WGL-6 (**a**), WGL-7 (**b**), and WGL-8 (**c**) at 5–60 mV s^{-1}

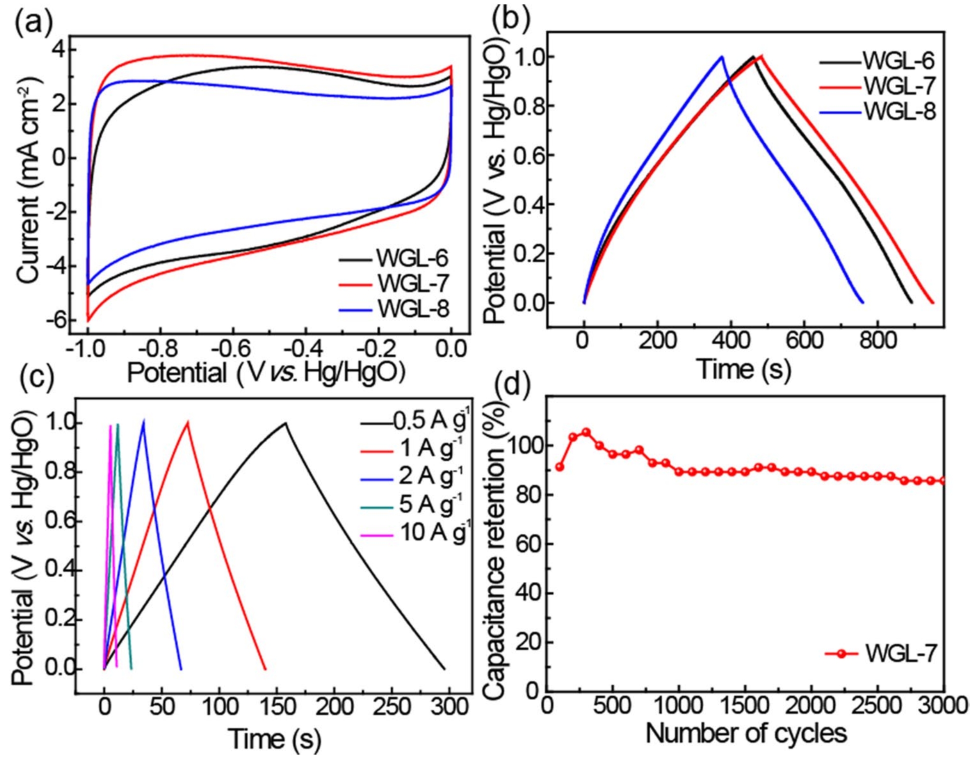

Fig.7 CV curves at 5 mV s^{-1} (**a**), GCD curves at 0.5 A g^{-1} (**b**) of WGL-6, WGL-7, and WGL-8; **c** GCD curves of the WGL-7 at 0.5–10A g^{-1} in a two-electrode system; **d** the capacitance retention of WGL-7

a prospective application because of their high specific surface area and abundant apertures, and WGL-7 would exhibit the best super capacitive performance.

The electrochemical properties of carbon materials were measured by cyclic voltammetry (CV) scans and galvanostatic charge–discharge (GCD) tests. Figure 6a–c showed the CV curves of WGL-6, WGL-7, and WGL-8 at 5–60 mV s^{-1}. All the curves exhibited the approximate rectangle feature, indicating that WGL-6, WGL-7, and WGL-8 showed typical electrochemical double layer capacitors (EDLC) behavior. Figure S2a-S2c gave the charge–discharge curves at 0.5–10 A g^{-1} of WGL-6, WGL-7, and WGL-8. All curves presented a symmetrical triangle, indicating that WGLs had good capacitance reversibility. Figure 7a compared the CV curves of WGL-6, WGL-7, and WGL-8 at 5 mV s $^{-1}$. A larger CV integrated area of WGL-7 indicated its better specific capacitance as supercapacitor electrode material. Figure 7b compared the charge–discharge curves of WGL-6, WGL-7, and WGL-8 at 0.5 A g^{-1}. The specific capacitances of WGL-6, WGL-7, and WGL-8 were calculated to 211, 236,

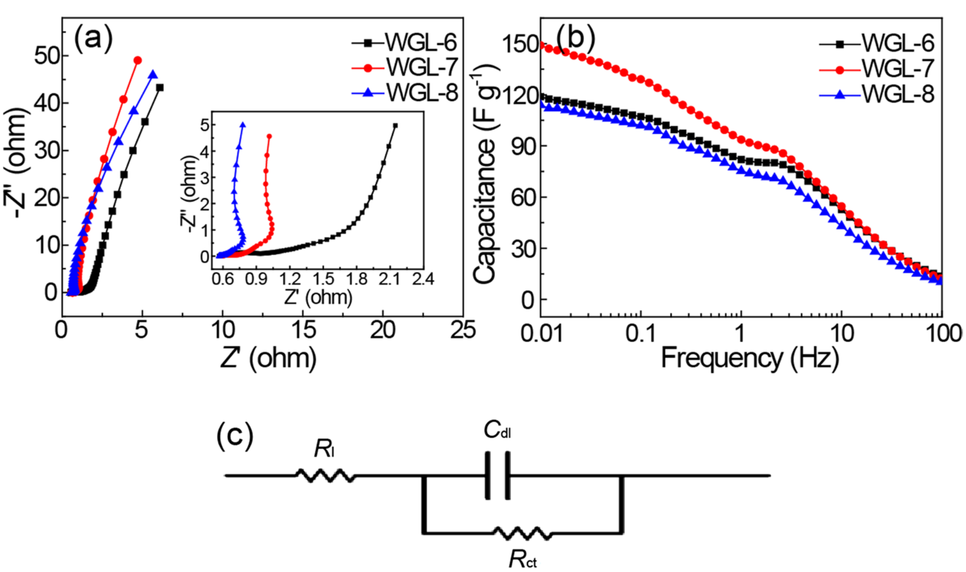

Fig. 8 Nyquist diagrams (**a**), the relationship of the specific capacitance and the frequency (**b**), and corresponding equivalent circuit (**c**) of WGL-6, WGL-7, and WGL-8. Inset in (**a**) showed the Nyquist plots in high-frequency region

and 185 F g^{-1}, respectively. These results demonstrated that WGL-7-modified electrodes displayed the highest capacitance at all current densities. When WGL-7-modified electrodes were applied in a two-electrode symmetric capacitor (Fig. 7c), its specific capacitance reached 57.2 F g^{-1} at 0.5 A g^{-1}, where the energy density was 31.8 W h kg^{-1} and the power density was 1003.5 W kg^{-1}. The cycle stability test of WGL-7 at 10 A g^{-1} was shown in Fig. 7d. After 3000 cycles of charge–discharge, the capacitance retention rate of WGL-7 remained still about 94.4%.

To understand their impedance behavior performance, electrochemical impedance spectroscopy (EIS) tests were performed. Nyquist diagrams of WGL-6, WGL-7, and WGL-8 were displayed in Fig. 8a. In the high-frequency range, all WGLs showed small semicircles and their equivalent series resistance (ESR) were all less than 0.1 Ω, illustrating the WGL-modified electrodes exhibited low charge-transfer resistance and negligible series resistance. In the low-frequency region, the straight line of WGL-7 showed the maximum slope compared to WGL-6 and WGL-8, indicating that WGL-7 was more potential in capacitive performance. Figure 8b gave the capacitance-frequency plots of WGL-6, WGL-7, and WGL-8. Specific capacitances of WGL-6, WGL-7, and WGL-8 at the low-frequency of 0.01 Hz were 119, 146, and 114 F g^{-1}, respectively. WGL-7 displayed the highest specific capacitance at the same frequency. The trend was in accordance with the results of CV and GCD tests. Nyquist diagrams can be fitted by the equivalent circuit shown in Fig. 8c.

4 Conclusion

In summary, walnut green peel was successfully converted into activated carbon materials WGLs by the carbonization and KOH activation. WGLs showed high specific surface areas with abundant aperture and structural defects, and were potential in supercapacitors. Among them, WGL-7 activated at 700 °C had the highest specific surface area (1404.3 m^2 g^{-1}) as well as modest oxygen doping and wettability. EIS tests also showed WGL-7 exhibited fast charge-transfer and potential application in capacitive performance. The capacitance of WGL-7-modified electrodes achieved 236 F g^{-1} at 0.5 A g^{-1} and showed excellent cycle stabilization in 6 M KOH electrolyte. The study demonstrated that converting walnut green peel into activated porous carbon as electrode materials for supercapacitor provided a potential avenue to reduce environmental pollution caused by walnut green peel and maximize its value.

Supplementary Information The online version contains supplementary material available at https://doi.org/10.1007/s13399-021-02103-7.

Author contribution Na Tian: conceptualization, validation, writing. Man Gao & Xiaoming Liu: methodology, resources. Tiantian Yang & Wenke Xie: visualization, formal analysis. Xuan-He Liu & Jing Wu: supervision.

Funding This work was supported by NSFC (21603194) and Fundamental Research Funds for the Central Universities (35842019057).

Declarations

Competing interest The authors declare no conflict of interest.

References

1. Thomas P, Lai CW, Bin-Johan MR (2019) Recent developments in biomass-derived carbon as a potential sustainable material for super-capacitor-based energy storage and environmental applications. J Anal Appl Pyrol 140:54–85. https://doi.org/10.1016/j.jaap.2019.03.021
2. Xu D, Cen HL (2021) A hybrid energy storage strategy based on multivariable fuzzy coordinated control of photovoltaic grid-connected power fluctuations. IET Renew Power Gener 15:1826–1835. https://doi.org/10.1049/rpg2.12152
3. Olabi AG (2017) Renewable energy and energy storage systems. Energy 136:1–6. https://doi.org/10.1016/j.energy.2017.07.054
4. Xu Q, Kobayashi T (2015) Advanced electrode materials for electrochemical capacitors. Adv Mater Clean Energy 7:194–215. https://doi.org/10.1201/b18287-10
5. Yan JJ, Zhu DZ, Lv YK, Xiong W, Liu MX, Gan LH (2020) Water-in-salt electrolyte ion-matched N/O codoped porous carbons for high-performance supercapacitors. Chin Chem Lett 31:579–582. https://doi.org/10.1016/j.cclet.2019.05.035
6. Goldfarb JL, Dou GL, Salari M, Grinstaff MW (2017) Biomass-based fuels and activated carbon electrode materials: an integrated approach to green energy systems. ACS Sustain Chem Eng 5:3046–3054. https://doi.org/10.1021/acssuschemeng.6b02735.s001
7. Lu MW, Huang Y, Chen C (2020) Cedarwood Bark-derived hard carbon as an anode for high-performance sodium-ion batteries. Energy Fuels 34:11489–11497. https://doi.org/10.1021/acs.energyfuels.0c01841
8. Zhou H, Zhou YM, Li L, Li YH, Liu XQ, Zhao P, Gao B (2019) Amino acid protic ionic liquids: multifunctional carbon precursor for N/S codoped hierarchically porous carbon materials toward supercapacitive energy storage. ACS Sustain Chem Eng 7:9281–9290. https://doi.org/10.1021/acssuschemeng.9b00279
9. Guna V, Ilangovan M, Prasad MGA, Reddy N (2017) Water hyacinth: a unique source for sustainable materials and products. ACS Sustain Chem Eng 5:4478–4490. https://doi.org/10.1021/acssuschemeng.7b00051
10. Shanmugapriya S, Surendran S, Lee YS, Selvan RK (2019) Improved surface charge storage properties of Prosopis juliflora (pods) derived onion–like porous carbon through redox-mediated reactions for electric double layer capacitors. Appl Sur Sci 492:896–908. https://doi.org/10.1016/j.apsusc.2019.06.147
11. Kobina SD, Kobina SE, Lv XM (2020) Application of biomass-derived nitrogen-doped carbon aerogels in electrocatalysis and

supercapacitors. Chem Electro Chem 7:3695–3712. https://doi.org/10.1002/celc.202000829
12. Liu GW, Qiu L, Deng H, Wang JB, Yao L, Deng LB (2020) Ultrahigh surface area carbon nanosheets derived from lotus leaf with super capacities for capacitive deionization and dye adsorption. Appl Surf Sci 524:146485. https://doi.org/10.1016/j.micromeso.2019.05.002
13. Pontiroli D, Scaravonati S, Magnani G, Fornasini L, Bersani D, Bertoni G, Milanese C, Girella A, Ridi F, Verucchi R, Mantovani L, Malcevschi A, Riccò M (2019) Super-activated biochar from poultry litter for high-performance supercapacitors. Micropor Mesopor Mat 285:161–169. https://doi.org/10.1016/j.micromeso.2019.05.002
14. Yang HF, Sun XY, Zhu H, Yu YM, Zhu QW, Fu ZX, Ta SW, Wang LX, Zhu HK, Zhang QT (2020) Nano-porous carbon materials derived from different biomasses for high performance supercapacitors. Ceram Int 46:5811–5820. https://doi.org/10.1016/j.ceramint.2019.11.031
15. Wang S, Lv L, Shen TR, Gan LH (2018) Research progress in preparation of biomass-derived mesoporous carbon materials. Modern Chemical Industry 38:23–28
16. Lian J, Xiong LS, Cheng R, Pang DQ, Tian XQ, Lei J, He R, Yu XF, Duan T, Zhu WK (2019) Ultra-high nitrogen content biomass carbon supercapacitors and nitrogen forms analysis. J Alloys Compd 809:151664. https://doi.org/10.1016/j.jallcom.2019.151664
17. Liu P, Cai WQ, Wei JH, Cai ZJ, Zhu MY, Han BW, Yang ZC, Chen JW (2019) Ultrafast preparation of saccharide-derived carbon microspheres with excellent dispersibility via ammonium persulfate-assisted hydrothermal carbonization. J Mater Chem A 32:1880–1885. https://doi.org/10.1039/c9ta05557f
18. Nie GD, Zhao XW, Jiang JM, Luan YX, Shi JL, Liu JM, Kou ZK, Wang J, Long YZ (2020) Flexible supercapacitor of high areal performance with vanadium/cobalt oxides on carbon nanofibers as a binder-free membrane electrode. Chem Eng J 402:126924. https://doi.org/10.1016/j.cej.2020.126294
19. Ouyang YH, Xing T, Chen YL, Zheng LP, Peng J, Wu C, Chang BB, Luo ZG, Wang XY (2020) Hierarchically structured spherical nickel cobalt layered double hydroxides particles grown on biomass porous carbon as an advanced electrode for high energy asymmetric supercapacitor. J Energy Storage 30:101454. https://doi.org/10.1016/j.est.2020.101454
20. Liu XB, Zou S, Liu KX, Lv C, Wu ZP, Yin YH, Liang TX, Xie ZL (2018) Highly compressible three-dimensional graphene hydrogel for foldable all-solid-state supercapacitor. J Power Sources 384:214–222. https://doi.org/10.1016/j.jpowsour.2018.02.087
21. Yang X, Jiang ZH, Fei BH, Ma JF, Liu XG (2018) Graphene functionalized bio-carbon xerogel for achieving high-rate and high-stability supercapacitors. Electrochim Acta 282:813–821. https://doi.org/10.1016/j.electacta.2018.06.131
22. Li FF, Wang XL, Sun RC (2017) A metal-free and flexible supercapacitor based on redox-active lignosulfonate functionalized graphene hydrogels. J Mater Chem A 5:20643–20650. https://doi.org/10.1039/c7ta03789a
23. Cui ZX, Gao XL, Wang JP, Yu JH, Dong HZ, Zhang Q, Yu LY, Dong LF (2018) Synthesis and supercapacitance of Co3O4 supported on porous carbon derived from wheat flour. ECS Meeting Abstracts 7:M161–M165. https://doi.org/10.1149/2.0141810jss
24. Karthikeyan K, Amaresh S, Lee SN, Sun XL, Aravindan V, Lee YG, Lee YS (2014) Construction of high-energy-density supercapacitors from pine-cone-derived high-surface-area carbons. Chem Sus Chem 7:1435–1442. https://doi.org/10.1002/cssc.201301262
25. Selvaraj AR, Muthusamy A, In-ho-Cho K-J, Senthil K, Prabakar K (2021) Ultrahigh surface area biomass derived 3D hierarchical porous carbon nanosheets electrodes for high energy density supercapacitors. Carbon 174:463–474. https://doi.org/10.1016/j.carbon.2020.12.052
26. Zhou XF, Wang BB, Jia ZR, Zhang XD, Liu XH, Wang KK, Xu BH, Wu GL (2021) Dielectric behavior of Fe3N@C composites with green synthesis and their remarkable electromagnetic wave absorption performance. J Colloid Interface Sci 582:515–525. https://doi.org/10.1016/j.jcis.2020.08.087
27. Fang ZM, Cao L, Lai FL, Kong DB, Du XS, Lin HJ, Lin ZD, Zhang P, Li W (2020) Carbon nano bowl array derived from a corncob sponge/carbon nanotubes/polymer composite and its electrochemical properties. Compos Sci and Technol 183:1007792. https://doi.org/10.1016/j.compscitech.2019.107792
28. Zhang LQ, Zhang YJ, Sha L, Ji XX, Chen HL, Zhao X (2021) Enhanced electrochemical performance of Si-carbon materials from Larch waste by filtration liquefaction residue process. Electrochim Acta 370:137813. https://doi.org/10.1016/j.electacta.2021.137813
29. Taer E, Apriwandi A, Ningsih YS, Taslim R, Riau I (2019) Preparation of activated carbon electrode from pineapple crown waste for supercapacitor application. Int J Electrochem Sci 14:2462–2475. https://doi.org/10.20964/2019.03.17
30. Du WM, Zhang ZR, Du LG, Fan XF, Shen ZW, Ren XR, Zhao YP, Wei CZ, Wei SH (2019) Designing synthesis of porous biomass carbon from wheat straw and the functionalizing application in flexible, all-solid-state supercapacitors. J Alloys Compd 797:1031–1040. https://doi.org/10.1016/j.jallcom.2019.05.207
31. Zhao YQ, Lu M, Tao PY, Zhang YJ, Gong XT, Yang Z, Zhang GQ, Li HL (2016) Hierarchically porous and heteroatom doped carbon derived from tobacco rods for supercapacitors. J Power Sources 307:391–400. https://doi.org/10.1016/j.jpowsour.2016.01.020
32. Zhu XQ, Yu S, Xu KT, Zhang Y, Zhang LM, Lou GB, Wu YT, Zhu EH, Chen H, Shen ZH, Bao BF, Fu SY (2018) Sustainable activated carbons from dead ginkgo leaves for supercapacitor electrode active materials. Chem Eng Sci 181:36–45. https://doi.org/10.1016/j.ces.2018.02.004
33. Seredych M, Jurcakova DH, Lu GQ, Bandosz TJ (2008) Surface functional groups of carbons and the effects of their chemical character, density and accessibility to ions on electrochemical performance. Carbon 46:1475–1488. https://doi.org/10.1016/j.carbon.2008.06.027
34. Surya K, Michael MS (2021) Hierarchical porous activated carbon prepared from biowaste of lemon peel for electrochemical double layer capacitors. Biomass Bioenergy 152:106175. https://doi.org/10.1016/j.biombioe.2021.106175
35. Yahya MD, Obayomi KS, Orekoya BA, Olugbenga AG, Akoh B (2020) Process evaluation study on the removal of Ni(II) and Cu(II) ions from an industrial paint effluent using kola nut pod as an adsorbent. J Disper Sci Technol 1-9. https://doi.org/10.1080/01932691.2020.1822178
36. Fang J, Guo D, Kang CX, Wan SY, Fu LK, Liu QM (2019) N, O-enriched hierarchical porous graphite carbon flake for high performance supercapacitors. J Electroanal Chem 851:113467. https://doi.org/10.1016/j.jelechem.2019.113467
37. Lin XX, Tan B, Peng L, Wu ZF, Xie ZL (2016) Ionothermal synthesis of microporous and mesoporous carbon aerogels from fructose as electrode materials for supercapacitors. J Mater Chem 4:4497–4505. https://doi.org/10.1039/c6ta00681g
38. Uddin MK, Nasar A (2020) Walnut shell powder as a low-cost adsorbent for methylene blue dye: isotherm, kinetics, thermodynamic, desorption and response surface methodology examinations. Sci Rep 10:7983. https://doi.org/10.1038/s41598-020-64745-3
39. Park D, Lim SR, Yun YS, Park JM (2007) Reliable evidences that the removal mechanism of hexavalent chromium by

natural biomaterials is adsorption-coupled reduction. Chemosphere 70:298–305. https://doi.org/10.1016/j.chemosphere.2007.06.007
40. Shen GZ, Yang AH, Zou GH (2016) Research progress on chemical constituents and biological activities of Qinglongyi. China J Chin Mater Med: 1–7
41. Li SJ, Han KH (2019) Preparation and electrochemical properties of algae-based super activated carbon based on "egg-box" structure. J of Mater Engine 47:97–104
42. Jiang WC, Li LY, Pan JQ, Senthil RA, Jin X, Cai JQ, Wang J, Liu XG (2019) Hollow-tubular porous carbon derived from cotton with high productivity for enhanced performance supercapacitor. J Power Sources 438:226936. https://doi.org/10.1016/j.jpowsour.2019.226936
43. Liang ZL, Yang Y, Li H, Liu LY, Shi ZC (2020) Lithium storage performance of hard carbons anode materials prepared by different precursors. J Electrochem 27:177–184
44. Rajesh M, Manikandan R, Park S, Kim BC, Cho WJ, Yu KH, Raj CJ (2020) Pinecone biomass-derived activated carbon: the potential electrode material for the development of symmetric and asymmetric supercapacitors. Int J Energy Res 44:8591–8605. https://doi.org/10.1002/er.5548
45. Lan DW, Chen MY, Liu YC, Liang QL, Tu WW, Chen YY, Liang JJ, Qiu F (2020) Preparation and characterization of high value-added activated carbon derived from biowaste walnut shell by KOH activation for supercapacitor electrode. J Mater Sci Mater Electron 31:18541–18553. https://doi.org/10.1007/s10854-020-04398-0
46. Wang C, Xiong Y, Wang HW, Sun QF (2018) All-round utilization of biomass derived all-solid-state asymmetric carbon-based supercapacitor. J Colloid Interface Sci 528:349–359. https://doi.org/10.1016/j.jcis.2018.05.103
47. Jiang LY, Han SOK, Pirie M, Kim HH, Seong YH, Kim H, Foord JS (2021) Seaweed biomass waste-derived carbon as an electrode material for supercapacitor. Energy Environ 32:1117–1129. https://doi.org/10.1177/0958305X19882398
48. Zhang W, Xu J, Hou D, Yin J, Liu D, He Y, Lin H (2018) Hierarchical porous carbon prepared from biomass through a facile method for supercapacitor applications. J Colloid Interf Sci 530:338–344. https://doi.org/10.1016/j.jcis.2018.06.076
49. Islam MA, Ong HL, Villagracia ARA, Halim KA, Ganganboina AB, Doong R-A (2021) Biomass–derived cellulose nanofibrils membrane from rice straw as sustainable separator for high performance supercapacitor. Ind Crops Prod. 170:113694. https://doi.org/10.1016/j.indcrop.2021.113694
50. Rajendiran R, Nallal M, Park KH, Li OL, Kim HJ, Prabakar K (2019) Mechanochemical assisted synthesis of heteroatoms inherited highly porous carbon from biomass for electrochemical capacitor and oxygen reduction reaction electrocatalysis. Electrochim Acta 317:1–9. https://doi.org/10.1016/j.electacta.2019.05.139
51. Ali AM, Supriya S, Chong KF, Essam SR, Algarni H, Maiyalagan T, Hegde G (2021) Superior supercapacitance behavior of oxygen self-doped carbon nanospheres: a conversion of Allium cepa peel to energy storage system. Biomass Convers Biorefinery 11:1311–1323. https://doi.org/10.1007/s13399-019-00520-3
52. Mohammed AA, Chen C, Zhu ZH (2019) Low-cost, high-performance supercapacitor based on activated carbon electrode materials derived from baobab fruit shells. J Colloid Interf Sci 538:308–319. https://doi.org/10.1016/j.jcis.2018.11.103
53. Shao YB, Xu LF, Hu ZY, Zhao GL, Li JQ, Gan QQ, Tang QQ, Dai W, Ouyang MG (2021) Pseudo-steady state of high-frequency resistance for polymer electrolyte membrane fuel cell: effect of in-plane heterogeneity. J Electrochem Soc 168:084509. https://doi.org/10.1149/1.1365141